

Resonant Raman effect in cinnabar

W. Imano, C. T. Simpson, W. M. Becker, and A. K. Ramdas

Department of Physics, Purdue University, West Lafayette, Indiana 47907

(Received 30 July 1979)

In α -HgS, cinnabar, grown by chemical vapor transport, a sharp photoluminescence feature is found at an energy $E(X_1) = 1.873$ eV. Absorption measurements show that this peak is due to resonance fluorescence associated with an electronic transition. When the Raman spectrum of such samples is excited with laser energy $\hbar\omega_L$ in the range 1.865–1.885 eV provided by a dye laser, new Raman lines appear at 21, 33.5, 67, and 101 cm^{-1} . These lines exhibit a pronounced resonance in the spectral dependence of their scattering intensity. The 33.5- and 67- cm^{-1} lines, for which we have a complete spectral dependence, show a resonance peak at $\hbar\omega_L = E(X_1)$ as well as for $\hbar\omega_L = E(X_1) +$ the phonon energy. The shape of their resonance curves agrees well with that predicted by the theory of the resonance Raman effect. These resonance curves also exhibit a peak at $\hbar\omega_L = E(Z_1) +$ the phonon energy, where $E(Z_1) = 1.870$ eV. The 33.5-, 67-, and 101- cm^{-1} Raman lines are ascribed to the first, second, and third harmonics of a Raman inactive A_2 (TO) mode, activated under resonance conditions as a result of a breakdown of the usual selection rules. The 21- cm^{-1} line can be interpreted as an "in-band resonant mode." The zone-center Raman-active phonons at 43 and 48 cm^{-1} , of A_1 and E symmetry, respectively, also show a resonance enhancement for $\hbar\omega_L = E(X_1)$.

I. INTRODUCTION

The trigonal form of mercury sulfide, cinnabar or α -HgS, is a wide band-gap semiconductor, which exhibits a pronounced band-edge dichroism,¹ a large birefringence,² remarkable optical activity,^{3,4} and one of the strongest acousto-optic effects observed.⁵ The luminescence of cinnabar has been studied both by electron-beam excitation⁶⁻¹⁴ and by above band-gap photoexcitation.¹⁵ Using hydrothermally grown as well as naturally occurring cinnabar, these groups have reported green, yellow, and red luminescence which they attribute to edge emission, impurity bands, and donor-acceptor pairs. In chemical vapor transport grown (CVT) mercury sulfide, excited by above band-gap radiation, we have reported¹⁶ features similar to those seen by the above authors. In addition, with below band-gap excitation, we observed new photoluminescence features ~ 0.4 eV below the band-gap, some of which are remarkably sharp. A detailed description of this photoluminescence spectrum will be reported in a separate publication.¹⁷

The zone-center optical phonons have been studied both by infrared reflectivity¹⁸⁻²¹ and by Raman scattering.^{21,22} Employing these two techniques, all the expected zone-center optical phonons have been identified.²³ The spectral dependence of the Raman scattering intensity has proved to be a valuable technique in the investigation of the electronic states in the crystal participating as intermediate states in Raman scattering.²⁴ For example, resonant Raman scattering has been observed due to free excitons in

Cu_2O ,²⁵ free and bound excitons in CdS,^{26,27} and band to band transitions in GaP.²⁸ Besides an enhancement of the Raman scattering, one may also encounter a breakdown of the usual selection rules as has been observed by Compaan and Cummins²⁵ in Cu_2O . Furthermore, in systems where the intermediate states are well characterized, resonant Raman scattering can provide information about the scattering process itself.²⁴ In the previous Raman scattering work by Zallen *et al.*²¹ and by Nusimovici and Meskaoui,²² only the 6328- \AA radiation from an He-Ne laser was used to excite the Raman spectrum.

In view of this, we have measured the Raman spectrum of cinnabar with exciting radiation ~ 0.4 eV below to ~ 0.1 eV above the band edge. In the course of this investigation we have observed a resonant enhancement near the band edge as well as near the sharp photoluminescence features. The band-edge work will be published separately. In this paper, we present our results of the Raman scattering when laser excitation is in the vicinity of the sharp features referred to above. Under these conditions, we observe resonances in the scattering cross sections of several Raman lines, some of which appear only with laser excitation in this range.

II. EXPERIMENTAL

The samples used in this investigation were grown using a modified CVT technique described by Faile.²⁹ Iodine and NH_4Cl were used as transport agents and growth runs of ~ 2 weeks yielded optically clear crystals with tabular habit having

dimensions of $\sim 1 \times 2 \times 0.3$ mm. The crystals were oriented with x-rays using the back-reflection Laue method and optically by using conoscopic figures. The largest face was the basal plane, $c\{0001\}$. For backscattering along the optic axis, c , the sample surfaces were as-grown, but for back-scattering perpendicular to the c -axis, a face parallel to the c -axis was prepared by grinding with successively finer grits of carborundum powder followed by polishing on a Rayvel cloth with a slurry of 1–5 μ chrome oxide.³⁰ Samples were cooled by immersion in pumped liquid helium or mounted on a cold finger of a three-window optical glass cryostat.³¹

Raman spectra were recorded with a Spex double monochromator³² equipped with 1800 grooves/mm holographic gratings, or a Jarrell-Ash double monochromator³³ incorporating 1180 grooves/mm gratings. The detection system consisted of a cooled RCA C31034-02 photomultiplier³⁴ together with the standard photon counting electronics.³⁵ For most experiments a ratemeter was used to produce a trace on an X-Y recorder while in some instances the spectra were multiscanned and stored in a multichannel analyzer.³⁶ The data were then transferred via paper tape to a digital computer for analysis. In the spectral region of interest, the throughput of the spectrometer was significantly greater for light polarized perpendicular rather than parallel to the grooves of the grating. When necessary the plane of polarization of the analyzed radiation was rotated to the horizontal with a mica half-wave plate in order to use the spectrometer with the maximum throughput.

The Raman spectrum was excited by radiation from a Spectra-Physics He-Ne laser,³⁷ a Jodon Engineering He-Ne laser,³⁸ or a Coherent Radiation dye laser³⁹ pumped by a Coherent Radiation Ar⁺ laser.⁴⁰ In order to scan the dye laser energies from ~ 1.85 to ~ 2.35 eV, we employed the following dyes: Rhodamine 560, Rhodamine 590, Rhodamine 610, and Rhodamine 640.⁴¹ To exclude the broad dye fluorescence and the plasma lines of the He-Ne laser, we used prisms, spatial filters, and angle-tuned dielectric filters in the output beam of the laser. We were also careful to exclude the intense specularly reflected light from our collection optics. The intensity of the Raman lines was normalized to the power of the laser as measured by a Coherent Radiation power meter.⁴²

The energy range over which we display our results in this paper is small (1.865–1.885 eV), and the absorption is flat and structureless except for an extremely weak feature ($\Delta\alpha \sim 1$ cm⁻¹) at 1.873 eV. Therefore the spectral response of the power meter, the transfer function of the spec-

trometer, the " λ^4 " correction, and the absorption and reflection of the sample could be justifiably neglected.

III. RESULTS AND DISCUSSION

Figure 1 displays the Raman spectrum of cinnabar recorded with 6328-Å radiation in the back-scattering geometry with the incident wavevector, \vec{k}_i , and the scattered wavevector, \vec{k}_s , propagating perpendicular to c . The sample was mounted on a cold finger held at liquid-helium temperature, the light was incident vertically polarized but the scattered light was not analyzed. The point group of cinnabar is D_3 ; its character table is exhibited in Table I. The lines in Fig. 1 are labeled according to the irreducible representations of D_3 , and as can be seen from Table I, only A_1 or E symmetry phonons are Raman active. There are three formula groups per unit cell and the 15 zone-center optical phonons transform as $2A_1 + 3A_2 + 5E$. The shifts of the Raman active phonons reported by Zallen *et al.*²¹ and by Nusimovici and Meskaoui²² are given in Table II along with our measured values. We see that all three sets of measurements are in agreement, although our values appear closer to those of Nusimovici and Meskaoui²² both in terms of the shifts of the Raman lines as well as the temperature dependence of the shifts.

Figure 2 exhibits the Raman and the photoluminescence spectrum at $T \sim 22$ K. (The temperature was determined by measuring the voltage of a light-emitting diode chip⁴³ mounted on the cold finger.) A broad luminescence, labeled B_2 at 1.78 eV dominates the spectrum and is accompanied on its high-energy side by two sharper luminescence features, labeled X_1 and X_2 in the figure, at 1.872 and 1.854 eV, respectively; at this temperature the halfwidth of X_1 is 3.7 meV and of X_2 is 6.6 meV. Luminescence features

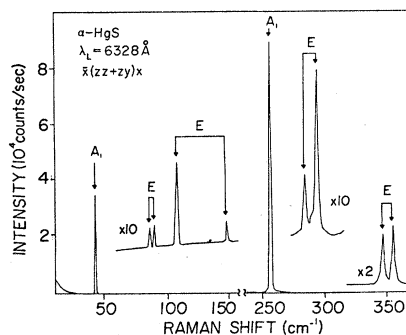


FIG. 1. Raman spectrum of cinnabar at liquid-helium temperature excited with ~ 35 mW of 6328-Å radiation.

TABLE I. Character table of D_3 and the zone-center optical phonons of cinnabar.^a

D_3	E	$2C_3$	$3C_2$	Basis functions	N_o	Raman active	Infrared active
A_1	1	1	1	$Z^2; X^2 + Y^2$	2	Yes	No
A_2	1	1	-1	Z	3	No	Yes
E	2	-1	0	$(X, Y); (X^2 - Y^2, -2XY); (YZ, -ZX)$	5	Yes	Yes

^a $X, Y,$ and Z are components of a polar vector field and N_o is the number of zone-center optical phonons.

are also seen between X_1 and X_2 but these are an order of magnitude weaker in intensity than X_1 or X_2 . A comprehensive discussion of luminescence, the excitation spectra and absorption spectra will be published separately.¹⁷ In the context of the resonant Raman scattering investigated in this work, it is of interest to discuss the absorption spectrum in the region of X_1 and X_2 shown in Fig. 3. The lower trace in Fig. 3 shows the X_1 photoluminescence when excited with 110 mW of 6400-Å radiation. The sample was immersed in pumped liquid helium; at this temperature (~2 K) the width of the luminescence is 2.6 meV. Centered at the peak of the X_1 luminescence is an absorption line whose width is approximately equal to that of the luminescence line. Within our detection limits, an absorption line corresponding to the X_2 photoluminescence was not observed. From this observation, we conclude that X_1 corresponds to resonance fluorescence and absorption where the transition is purely electronic. When the energy of the incident photon is near an electronic transition in the crystal, we expect a resonant enhancement of the Raman intensities. For this

reason, we examined the behavior of the Raman spectrum when the laser energy was scanned through X_1 employing a dye laser.

In Fig. 4 we compare the Raman spectrum excited with radiation of energy, $\hbar\omega_L$, coincident with the energy of X_1 , $E(X_1)$, with that when $\hbar\omega_L \gg E(X_1)$. The spectrum labeled "A" shows that, on resonance, two new Raman lines at 48.5 and 33.5 cm^{-1} appear, with the latter dominating the spectrum. This is in striking contrast to the off-resonance case where only the 43- cm^{-1} line appears. Spectra A and B were excited with 56 mW of 6619-Å radiation and 30 mW of 6400-Å radiation, respectively.

In Fig. 5, we plot the energies of the Raman and luminescence lines as a function of the exciting laser energy $\hbar\omega_L$. Such a plot allows one to graphically distinguish the Raman lines from the luminescence lines, since the latter appear at the same energy, independent of $\hbar\omega_L$, whereas the former have constant energy shifts from $\hbar\omega_L$. We thus observe that a number of Raman lines occur with shifts in the range 20–150 cm^{-1} , many of which are observed only under the resonant

TABLE II. First-order Raman lines of cinnabar.

Mode	Zallen <i>et al.</i> ^a		Nusimovici and Meskaoui ^b		Present work		
	300 K	90 K	300 K	90 K	300 K	80 K	20 K
A_1	45	42	42	44	42.0	42.4	42.9
E	TO		42	38			
	LO		42	49			
E	TO	88	85	87	85.0	86.5	86.9
	LO	91	88	91	88.3	90.3	90.9
E	TO	106	106	106	103.2	108.5	109.3
	LO	146	146	145	145.6	148.5	149.4
A_1	256	254	255	259	254.4	256.2	256.5
E	TO	283	282	283	283.5	283.8	284.4
	LO	290	289	289	289.9	293.3	293.8
E	TO	345	341	343	344.5	345.6	346.2
	LO	353	349	351	353.0	353.6	354.2

^a See Ref. 21.

^b See Ref. 22.

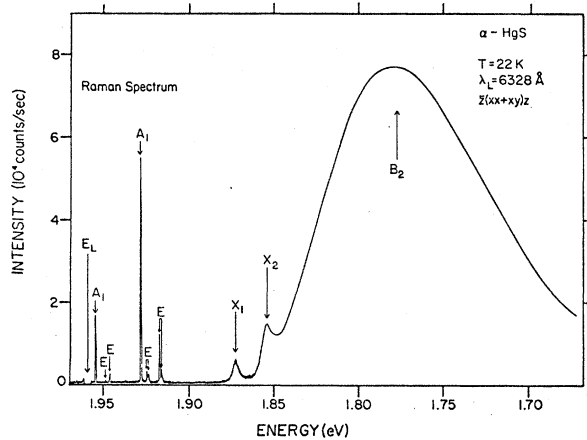


FIG. 2. The Raman spectrum and photoluminescence spectrum of cinnabar at 22 K excited with ~ 5 mW of 6328- \AA radiation.

conditions fulfilled in this experiment; lines 1, 2, 5, and 6 have not been reported previously in the Raman spectrum. In contrast to the other Raman lines, line 1 at 21 cm^{-1} is distinctly broader with a half width of 5.9 cm^{-1} . Lines 5 and 6 appear to be 1st and 2nd overtones of line 2 at 33.5 cm^{-1} . Line 3 at 43.3 cm^{-1} has been identified by Zallen *et al.*²¹ as a zone-center optical phonon of A_1 symmetry; under nonresonant conditions this is the most prominent line among those with shifts less than 250 cm^{-1} . Line 4 at 48.5 cm^{-1} has been

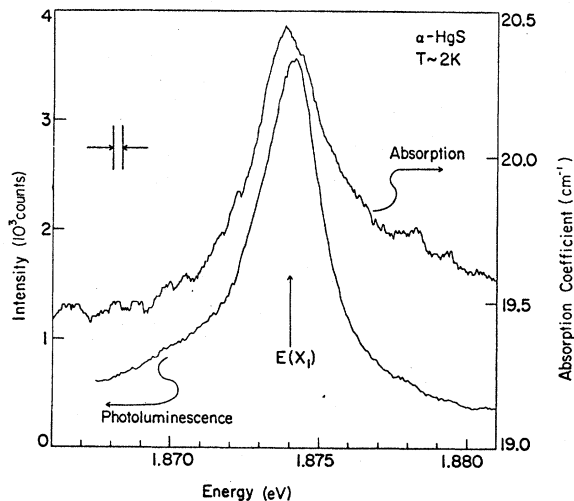


FIG. 3. The photoluminescence (lower trace) and optical absorption (upper trace) of the X_1 line of cinnabar at ~ 2 K. The photoluminescence was excited with 110 mW of 6400- \AA radiation. The half width of the photoluminescence line is 2.6 meV and that of the optical absorption line is 3.1 meV.

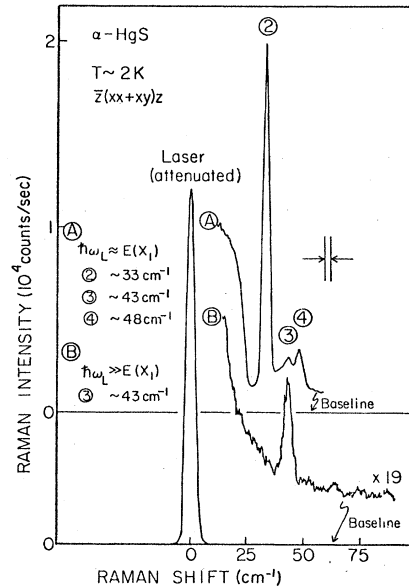


FIG. 4. A comparison of the Raman spectrum of cinnabar at ~ 2 K (A) "in resonance," with the exciting laser energy, $\hbar\omega_L$, close to $E(X_1)$, and (B) "off resonance," i.e., $\hbar\omega_L \gg E(X_1)$. The "in resonance" spectrum (A) was excited with 56.5 mW of 6619- \AA radiation and the "off resonance" spectrum (B) was excited with 30 mW of 6400- \AA radiation.

identified by Marqueton *et al.*²⁰ and by Nusimovici and Meskaoui²² as an LO component of an E mode.

In order to display the resonance Raman effect of the lines discussed above, we plot in Figs. 6–10 the normalized intensities of the Raman lines as a function of $\hbar\omega_L$. Figure 6 displays the Raman intensity of line 2 at 33.5 cm^{-1} in the spectral region near X_1 . Two prominent and sharp peaks occur in the scattering intensity; one at $\hbar\omega_L = E(X_1)$ and the other at $\hbar\omega_L = E(X_1) + \hbar\Omega_2$, where $\hbar\Omega_2$ is the energy of the phonon involved $= 33.5\text{ cm}^{-1}$. The enhancement that occurs when $\hbar\omega_L$, the incident photon energy, or $\hbar\omega_s$, the scattered photon energy, is equal to an electronic transition in the crystal will be referred to as an "in resonance" or "out resonance," respectively. We attribute the shoulder on the high-energy side of $\hbar\omega_L = E(X_1)$ to an "out resonance" due to a level labeled " Z_1 " at 1.870 eV. Luminescence from this level is weak but appears as a shoulder on the photoluminescence of X_1 in Fig. 3. The solid line in the figure is a theoretical fit to the data based on considerations given below. The resonance behavior of the 67- cm^{-1} line, the 1st overtone of the 33- cm^{-1} line, is displayed in Fig. 7 and shows "in" and "out" resonance peaks due to X_1 and an out resonance due to Z_1 . Note that due to the larger phonon energy, the out resonance

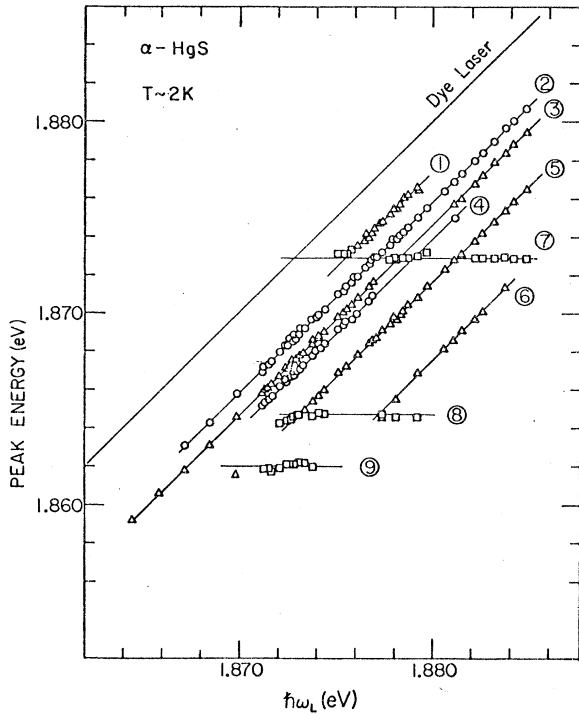


FIG. 5. The peak energy of the Raman and photoluminescence lines as a function of dye laser energy, $\hbar\omega_L$, for $1.865 \leq \hbar\omega_L \leq 1.885$ eV. The Raman lines labeled 1-6 have constant energy shifts with respect to $\hbar\omega_L$, whereas the luminescence lines labeled 7-9 are observed at a constant energy, independent of $\hbar\omega_L$. The Raman shifts of lines 1-6 are 21.0, 33.5, 43.3, 48.5, 67.4, and 100.7 cm^{-1} , respectively. The energies of the luminescence lines 7-9 are 1.873, 1.865, and 1.862 eV, respectively. Note that line 7 is referred to as X_1 in the text.

due to Z_1 is well resolved from the other peaks, in contrast to the similar peak in Fig. 6. Again, the solid line is a theoretical fit, to be discussed below. In Fig. 8 the scattering intensity of the 48- cm^{-1} line is plotted as a function of $\hbar\omega_L$. Only one prominent peak, that due to an in resonance from the X_1 level, is observed; the shape of the resonance shows a marked asymmetry. Figure 9 displays the scattering intensity of the 43- cm^{-1} line; it clearly shows a peak at $\hbar\omega_L = E(X_1)$, although the enhancement is only a factor of 4 over the nonresonant intensity. Its resonance behavior appears similar to that of the 48- cm^{-1} line and also exhibits asymmetry in the shape of the resonance. In Fig. 10 we exhibit the spectral dependence of the scattering intensity for the 21- cm^{-1} line. For $\hbar\omega_L < 1.875$ eV, the X_1 luminescence is strong and obscures the Raman line.

In a third-order perturbation treatment of Raman

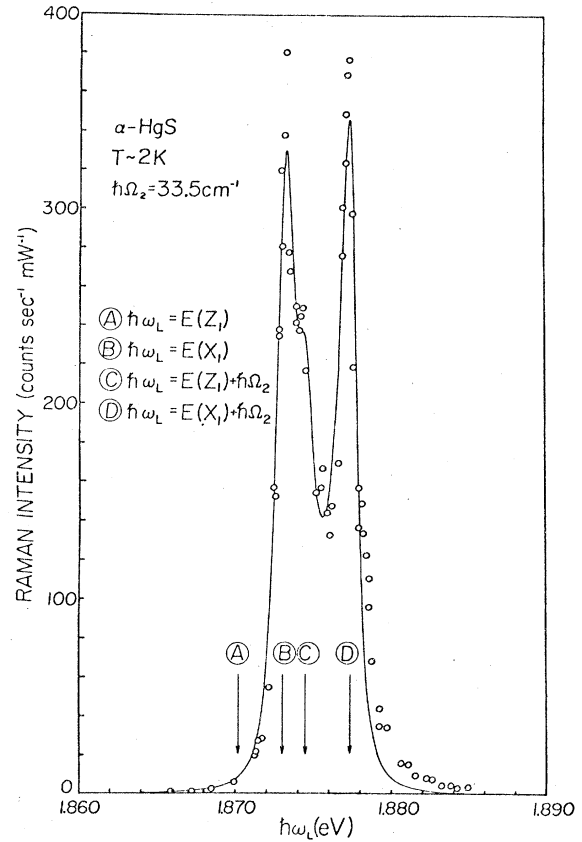


FIG. 6. The intensity of the 33- cm^{-1} Raman line as a function of dye laser energy, $\hbar\omega_L$. Note that the "in resonance" at $\hbar\omega_L = E(X_1)$ and the "out resonance" at $\hbar\omega_L = E(X_1) + \hbar\Omega_2$ are sharp, well-defined peaks. The solid line is a nonlinear least-squares fit to the data using Eq. (2). See Table III for the parameters used in the fit.

scattering in a semiconductor, one can expect large resonant enhancements in the scattering intensities when the incident or scattered photon is equal to an electronic transition to an intermediate state of the crystal. For example, Loudon⁴⁴ has treated Raman scattering mediated by free-electron and hole states, whereas Ganguly and Birman⁴⁵ have considered Raman scattering in insulators with intermediate exciton states. Consistent with these treatments, the spectral dependence of the scattering intensity can be written as

$$I(\Omega, E_L, E_S; E_i) = \frac{A_i}{(E_L - E_i)^2 + \gamma_i^2} + \frac{B_i}{(E_S - E_i)^2 + \Gamma_i^2}, \quad (1)$$

where Ω is the phonon frequency, E_L is the incident photon (laser) energy, E_S is the scattered

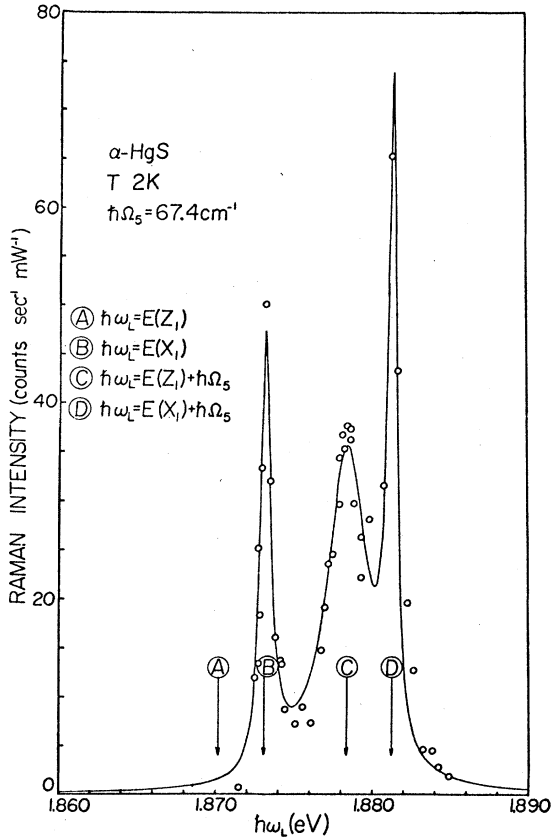


FIG. 7. The intensity of the 67-cm⁻¹ Raman line as a function of dye laser energy, $\hbar\omega_L$. In addition to the sharp, well-defined "in" and "out" resonances at $\hbar\omega_L = E(X_1)$ and $\hbar\omega_L = E(X_1) + \hbar\Omega_5$, there is a third, well-defined peak. This peak is ascribed to an "out resonance" of an energy state at 1.870 eV. The solid line is a non-linear least-squares fit to the data using Eq. (2). See Table III for the parameters used.

photon energy, E_i is the energy of the i th intermediate state; Γ_i and γ_i are damping parameters introduced here phenomenologically. The solid curve in Fig. 6 is a fit of the form

$$I = I(\Omega, E_L, E_S; E(X_1)) + I(\Omega, E_L, E_S; E(Z_1)). \quad (2)$$

Implicit in this expression is the assumption of no interference between terms involving the X_1 or Z_1 states. We introduce this assumption for simplicity. The fit was made using a nonlinear least-squares routine which minimized the mean-square errors. The parameters are exhibited in Table III. From the figure it is apparent that the solid curve agrees quite well with the experimental data, although the absence of the in resonance term for the Z_1 state is puzzling, since in both second-order⁴⁶ and third-order perturbation^{44,45} approaches to Raman scattering, the in resonance

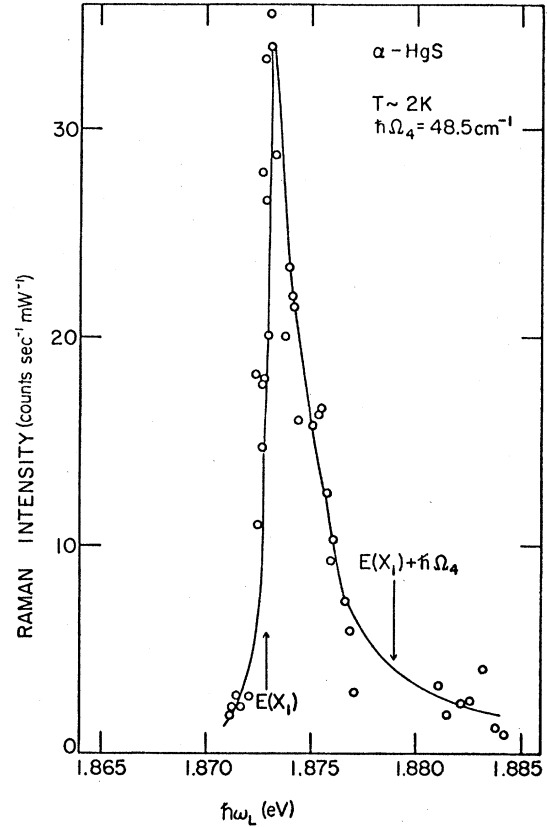


FIG. 8. The intensity of the 48-cm⁻¹ Raman line as a function of dye laser energy $\hbar\omega_L$. The solid line is drawn for clarity.

is always present. That the state Z_1 contributes in the out resonance only is seen more clearly in Fig. 7. Owing to the larger phonon energy the out resonance due to the Z_1 state is clearly resolved. The solid curve is a fit using Eq. (2) and the parameters given in Table III. Here, as in the 33-cm⁻¹ phonon, the in resonance due to Z_1 is noticeably absent. Qualitatively, the resonance behavior of the 43- and 48-cm⁻¹ phonons as shown in Figs. 8 and 9 exhibits an in resonance due to X_1 and a weaker or absent out resonance due to X_1 or Z_1 . A curve of the form of Eq. (1) yields a poor fit due mainly to the asymmetry in the resonance curve.

We do not attempt a detailed discussion of the resonance behavior of the 21-cm⁻¹ line since our data are incomplete, although it is apparent that there is at least an out resonance. For $\hbar\omega_L < 1.875$ eV the X_1 luminescence dominates and obscures this line, as mentioned above.

Although the resonance enhancement of the phonons is striking and appears to fall within the

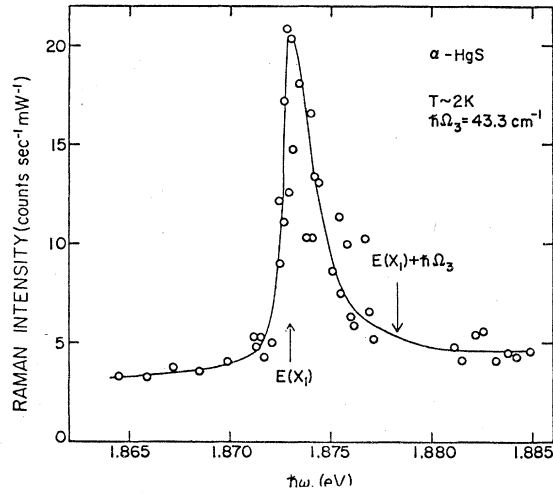


FIG. 9. The intensity of the 43-cm⁻¹ Raman line as a function of dye laser energy $\hbar\omega_L$. This line can be seen away from resonance. The solid line is drawn for clarity.

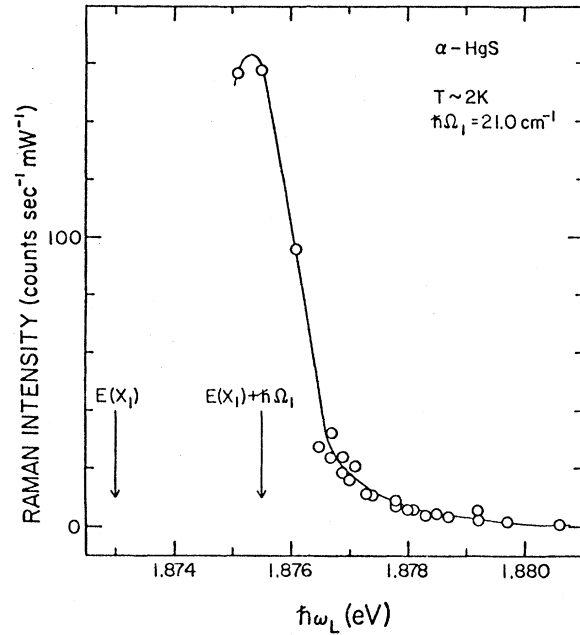


FIG. 10. The intensity of the 21-cm⁻¹ Raman line as a function of dye laser energy $\hbar\omega_L$. The solid line is drawn for clarity.

framework of the theory of resonance Raman scattering, the lack of specific information concerning X_1 has hindered our complete understanding of the resonant Raman process. Using the CVT technique, it is difficult to exclude impurities due to the transport agent or to include additional dopants. Because of the phase transition at 618 ± 2 K,⁴⁷ doping by a diffusion process is slow. Also, in our experience inclusions in the samples and the sample size prevented us from making reliable polarization measurements which are useful in symmetry assignments. We have attempted to correlate the X_1 luminescence with a specific chemical impurity by a mass spectrographic analysis of samples from two growth runs with similar morphological features

but only one exhibiting the luminescence.¹⁷ The analysis yielded iodine in both runs at the level of 10^{19} cm⁻³; many other impurities such as Na and Cl were found in trace concentrations. However, no clue could be established as to the nature of the X_1 luminescence center.

Since significant amounts of impurities are present, it should not be surprising if localized modes or perturbed lattice modes appear in the Raman spectrum. We suspect that the 21-cm⁻¹ line is a mode of such an origin, since it has not been reported previously in either the Raman or

TABLE III. Parameters obtained from nonlinear least-squares fit.

Parameters	Resonance of 33-cm ⁻¹ mode	Resonance of 67-cm ⁻¹ mode
$E(X_1)$	1.873 eV	1.873 eV
$A(X_1)$	4.48×10^{-5}	5.37×10^{-6}
$\Gamma(X_1)$	0.41 meV	0.34 meV
$B(X_1)$	1.64×10^{-4}	1.50×10^{-5}
$\gamma(X_1)$	0.67 meV	0.51 meV
$E(Z_1)$	1.870 eV	1.870 eV
$A(Z_1)$	0	0
$\Gamma(Z_1)$		
$B(Z_1)$	2.05×10^{-4}	6.48×10^{-5}
$\gamma(Z_1)$	1.01 meV	1.37 meV
$\hbar\Omega$	4.04 meV	8.00 meV

infrared spectrum. A calculation of the phonon spectrum by Nusimovici and Gorre²² reveals no gap in the phonon spectrum below 150 cm⁻¹ and hence a low frequency gap mode does not seem likely. However, a local mode with its frequency lying within the band of frequencies of the intrinsic phonon, i.e., an "in-band resonant" mode is a possible interpretation of this line.⁴⁸

An infrared-active, Raman-inactive, normal mode at 33 cm⁻¹ has been deduced previously from the reststrahlen spectra and has been identified as an A₂ (TO) mode.^{20,21} It is possible that the Raman lines at 33, 67, and 101 cm⁻¹ are the fundamental and the first and second overtones of this A₂ (TO) mode acquiring Raman activity by a breakdown of the usual selection rules near resonance. However, the identification of this phonon as a TO mode implies a phonon propagation direction perpendicular to the *c*-axis, whereas we employ a back-scattering geometry parallel to this direction. From the usual wave vector selection rules this geometry selects a phonon propagating parallel to the *c* axis. However, due

to the high refractive index of the material ($n_o = 2.90$, $n_e = 3.26$ at 6200 Å) the reflection coefficient is rather large, and a reflection of the incident or the scattered light off the back surface of the sample can very well result in forward scattering along the *c* axis. This would easily allow the participation of a phonon propagating perpendicular to the *c* axis. The 48-cm⁻¹ line has been identified previously as an *E* (LO) mode also implying a phonon propagation direction perpendicular to the *c* axis, further confirming our argument above.

ACKNOWLEDGMENTS

We are indebted to Dr. S. P. Faile for supplying the crystals used in this investigation. Our thanks are due to Dr. R. J. Briggs who participated in the preliminary work on the Raman scattering of cinnabar. This work was supported by the NSF-MRL Program No. DMR 77-23798 and the National Science Foundation Grant No. DMR 77-27248.

-
- ¹R. Zallen, in *II-VI Semiconducting Compounds*, edited by D. G. Thomas (Benjamin, New York, 1967), p. 877.
- ²W. L. Bond, G. D. Boyd, and H. L. Carter, Jr., *J. Appl. Phys.* **38**, 4090 (1967).
- ³B. Ayrault, F. Lefin, H. Langlois, Y. Toudic, and J. F. Palmier, *Opt. Commun.* **5**, 239 (1972).
- ⁴H. Langlois, B. Ayrault, F. Lefin, and Y. Toudic, *Phys. Status Solidi B* **60**, 821 (1973).
- ⁵J. Sapriel, *Appl. Phys. Lett.* **19**, 533 (1971).
- ⁶J. P. Noblanc, J. Loudette, and G. Duraffourg, *Solid State Commun.* **5**, 803 (1967).
- ⁷G. Massé, J. P. Aicardi, J. P. Leyris, C. Butti, and F. Bombré, *C. R. Acad. Sci., Ser. B*, **278**, 85 (1974).
- ⁸G. Massé, J. P. Aicardi, and F. Bombré, *C. R. Acad. Sci. Ser. B* **279**, 669 (1974).
- ⁹J. P. Aicardi, G. Massé, and M. Egée, *Phys. Status Solidi A* **32**, 701 (1975).
- ¹⁰J. P. Aicardi, J. P. Leyris, G. Massé, and C. Butti, *C. R. Acad. Sci. Ser. B* **284**, 57 (1977).
- ¹¹J. P. Aicardi, J. P. Leyris, and G. Massé, *J. Lumin.* **16**, 201 (1978).
- ¹²J. P. Aicardi, J. P. Leyris, and G. Massé, *Phys. Status Solidi A* **39**, 125 (1977).
- ¹³G. Massé, J. P. Aicardi, and J. P. Leyris, *Phys. Status Solidi A* **43**, 191 (1977).
- ¹⁴G. Massé, J. P. Aicardi, and J. P. Leyris, *J. Lumin.* **17**, 29 (1978).
- ¹⁵G. G. Roberts and R. Zallen, *J. Phys. C* **4**, 1890 (1971).
- ¹⁶C. T. Simpson, W. I. Imano, W. M. Becker, and S. P. Faile, *Solid State Commun.* **28**, 39 (1978).
- ¹⁷C. T. Simpson, W. Imano, and W. M. Becker (unpublished).
- ¹⁸H. Poulet and J. P. Mathieu, *C. R. Acad. Sci., Ser. B*, **270**, 708 (1970).
- ¹⁹J. Barcelo, M. Galtier, and A. Montaner, *C. R. Acad. Sci. Ser. B* **274**, 1410 (1972).
- ²⁰Y. Marqueton, B. Ayrault, E. A. Decamps, and Y. Toudic, *Phys. Status Solidi B* **60**, 809 (1973).
- ²¹R. Zallen, G. Lucovsky, W. Taylor, A. Pinczuk, and E. Burstein, *Phys. Rev. B* **1**, 4058 (1970).
- ²²M. A. Nusimovici and A. Meskaoui, *Phys. Status Solidi B* **58**, 121 (1973).
- ²³M. A. Nusimovici and G. Gorre, *Phys. Rev. B* **8**, 1648 (1973).
- ²⁴R. M. Martin and L. M. Falicov, in *Light Scattering in Solids*, edited by M. Cardona (Springer, New York, 1975), p. 79.
- ²⁵A. Compaan and H. Z. Cummins, *Phys. Rev. Lett.* **31**, 41 (1973).
- ²⁶R. M. Martin and T. C. Damen, *Phys. Rev. Lett.* **26**, 86 (1971).
- ²⁷P. J. Colwell and M. V. Klein, *Solid State Commun.* **8**, 2095 (1970).
- ²⁸M. I. Bell, R. N. Tyte, and M. Cardona, *Solid State Commun.* **13**, 1833 (1973).
- ²⁹S. P. Faile, *J. Cryst. Growth* **43**, 129 (1978). See also M. M. Kreitman, S. P. Faile, C. W. Litton, and D. C. Reynolds, in *Proceedings of the International Conference on the Optical Properties of Highly Transparent Solids*, edited by S. S. Mitra and B. Bendow (Plenum, New York, 1975), p. 179.
- ³⁰Rayvel cloth and chrome oxide, Buehler Ltd., 2120 Greenwood St., Evanston, IL 60204.
- ³¹P. Fisher, W. H. Haak, E. J. Johnson, and A. K. Ramadas, in *Proceedings of the Eighth Symposium on the Art of Glassblowing* (The American Scientific Glass Blowers Society, Wilmington, Del., 1963), p. 136. The immersion cryostat used in the present paper is a

- modified version designed by R. J. Briggs.
- ³²Model 14018, Spex Industries, Inc., 3880 Park Avenue, Metuchen, N.J. 08840.
- ³³Model 25-100, Jarrell-Ash Division, 590 Lincoln St., Waltham, MA 02154.
- ³⁴Model C31034-02, RCA, Electronic Components Division, Harrison, N.J. 07029.
- ³⁵Model 9301 Preamplifier, Model 9302 Amplifier-Discriminator, Model 9349 Ratemeter, Ortec Incorporated, 100 Midland Road, Oak Ridge, TN 37830.
- ³⁶ND 1200 Analyzer System, Nuclear Data, Inc., Golf and Meacham Roads, Schaumburg, IL 60172.
- ³⁷Model 125, Spectra Physics, 1250 W. Middlefield Rd., Mountain View, CA 94040.
- ³⁸Model HN-7, Jodon Engineering Associates, Inc., 145 Enterprise Dr., Ann Arbor, MI 48103.
- ³⁹Model 490, Coherent Radiation, 3210 Porter Dr., Palo Alto, CA 94304.
- ⁴⁰Model CR-10U, Coherent Radiation, 3210 Porter Dr., Palo Alto, CA 94304.
- ⁴¹Exciton Chemical Co., Inc., 5760 Burkhardt Road, Dayton, OH 45431.
- ⁴²Model 212, Coherent Radiation, 3210 Porter Dr., Palo Alto, CA 94304.
- ⁴³B. F. Griffing and S. A. Shivashankar, *Rev. Sci. Instrum.* 48, 1225 (1977).
- ⁴⁴R. Loudon, *Proc. R. Soc. London, Ser. A*, 275, 218 (1963).
- ⁴⁵A. K. Ganguly and J. L. Birman, *Phys. Rev.* 162, 806 (1967).
- ⁴⁶G. Placzek, in *Handbuch der Radiologie*, edited by E. Marx (Akademische Verlagsgesellschaft, Leipzig, 1934), Vol. VI, Pt. 2, p. 205.
- ⁴⁷G. Kullerud, *Carnegie Inst. Washington, Yearb.*, Vol. 64, 1965, p. 193; F. W. Dickson and G. Tunell, *Am. Mineral.* 44, 471 (1959).
- ⁴⁸See, for example, A. S. Barker and A. J. Sievers, *Rev. Mod. Phys.* 47, Supplement No. 2, S1 (1975).